

Irreversibility, Loschmidt Echo, and Thermodynamic Uncertainty Relation

Yoshihiko Hasegawa*

Department of Information and Communication Engineering,
Graduate School of Information Science and Technology,
The University of Tokyo, Tokyo 113-8656, Japan

(Dated: February 28, 2025)

Entropy production characterizes irreversibility. This viewpoint allows us to consider the thermodynamic uncertainty relation, which states that a higher precision can be achieved at the cost of higher entropy production, as a relation between precision and irreversibility. In this study, we show that the precision of arbitrary counting observable in continuous measurement of quantum Markov processes is bounded from below by Loschmidt echo, representing the irreversibility of quantum dynamics. The obtained relation can be viewed as a quantum analog of thermodynamic uncertainty relation. Based on a total variation distance, we obtain that the distance between the probability distributions of counting observables is bounded from above by the Loschmidt echo.

Introduction.—The thermodynamic uncertainty relation (TUR) [1–17] (see [18] for a review) provides a universal relation between precision and thermodynamic cost. It states that $\|\mathcal{J}\|^2/\langle\mathcal{J}\rangle^2 \geq 2/\langle\sigma\rangle$, where $\langle\mathcal{J}\rangle$ and $\|\mathcal{J}\|$ are the mean and standard deviation, respectively, of a current observable \mathcal{J} , and σ is the mean of the entropy production. TUR indicates that a higher precision can be achieved at the cost of higher entropy production. The entropy production quantifies the irreversibility of the system. Let $\mathcal{P}_F(\Gamma)$ be the probability for observing a trajectory Γ in the forward process, and $\mathcal{P}_R(\bar{\Gamma})$ be the probability for observing a time-reversed trajectory $\bar{\Gamma}$ in the reversed process. Then, the entropy production is defined by a log-ratio between $\mathcal{P}_F(\Gamma)$ and $\mathcal{P}_R(\bar{\Gamma})$ [Fig. 1(a)]: $\sigma = \ln [\mathcal{P}_F(\Gamma)/\mathcal{P}_R(\bar{\Gamma})]$. This relation provides a viewpoint that TUR is a consequence of irreversibility, i.e., the larger the extent of irreversibility, the higher the precision of a thermodynamic machine.

In Newtonian dynamics, despite microscopic reversibility, irreversibility emerges due to the chaotic nature of many-body systems. For chaotic systems, even considering reversed dynamics by reversing the sign of the momenta, an infinitely small perturbation applied to the state produces an exponential divergence from the original reversed dynamics, indicating that it is impossible to achieve such reversed dynamics in reality. Thus, the extent of irreversibility can be evaluated through the extent of chaos, which is often quantified by the Lyapunov exponent in classical dynamics. The Loschmidt echo [19–21] is an indicator for the effect of small perturbations applied to the Hamiltonian in quantum systems. It can be viewed as a quantum analog of the Lyapunov exponent. Consider an isolated quantum system. Given an initial pure state $|\Psi(0)\rangle$, with Hamiltonian H and perturbed Hamiltonian H_* , the Loschmidt echo η is defined by

$$\eta \equiv |\langle\Psi(0)|e^{iH_*\tau}e^{-iH\tau}|\Psi(0)\rangle|^2. \quad (1)$$

Equation (1) evaluates the fidelity between two states, $e^{-iH\tau}|\Psi(0)\rangle$ and $e^{-iH_*\tau}|\Psi(0)\rangle$, at time $t = \tau$, where $\tau > 0$ [Fig. 1(b)]. These states are generated through

the forward time evolution induced by H and H_* , respectively. Alternatively, Eq. (1) can be viewed as the fidelity between $|\Psi(0)\rangle$ and $e^{iH_*\tau}e^{-iH\tau}|\Psi(0)\rangle$ at $t = 0$, where the latter state is obtained by applying the forward time evolution by H and the subsequent reversed time evolution by H_* to $|\Psi(0)\rangle$ [Fig. 1(c)]. The second interpretation provides a natural extension to classical irreversibility. In this Letter, we show that the precision of any counting observable in continuous measurement of quantum Markov processes is bounded from below by the Loschmidt echo. This relation can be viewed as a quantum extension of classical TURs. It is worth noting that the obtained quantum TUR holds for any continuous measurement, which has not been achieved for previous quantum TURs [22–32]. Besides, we obtain an inequality relation for the total variation distance between counting observables of the original and perturbed dynamics, where the upper bound consists of Loschmidt echo.

Results.—We consider a quantum Markov process described by a Lindblad equation [33, 34]. Let $\rho_S(t)$ be a density operator at time t in the principal system S . The time evolution of $\rho_S(t)$ is governed by

$$\dot{\rho}_S = \mathcal{L}\rho_S \equiv -i[H_S, \rho_S] + \sum_{m=1}^M \mathcal{D}(\rho_S, L_m), \quad (2)$$

where $\dot{\bullet}$ is the time derivative, \mathcal{L} is a Lindblad super-operator, H_S is a Hamiltonian, $\mathcal{D}(\rho_S, L) \equiv [L\rho_S L^\dagger - \{L^\dagger L, \rho_S\}/2]$ is a dissipator, and L_m ($1 \leq m \leq M$ with M being the number of L_m) is the m th jump operator ($[\bullet, \bullet]$ and $\{\bullet, \bullet\}$ denote the commutator and anticommutator, respectively). Note that H_S is different from the total Hamiltonian H , which induces unitary time evolution in the total system. For a sufficiently small-time interval Δt , the Lindblad equation of Eq. (2) admits the Kraus representation $\rho_S(t + \Delta t) =$

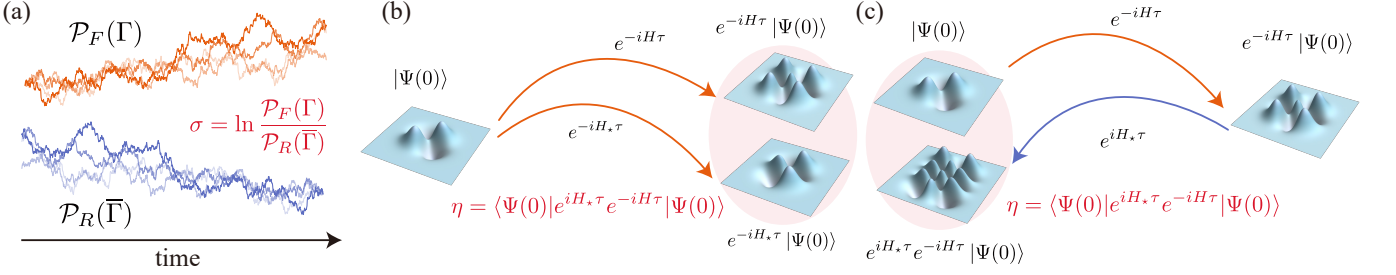


FIG. 1. Quantification of irreversibility. (a) Entropy production σ in classical Markov processes, defined by a log-ratio between $P_F(\Gamma)$, the probability for observing a trajectory Γ in the forward process, and $P_R(\bar{\Gamma})$, the probability for observing a time-reversed trajectory $\bar{\Gamma}$ in the reversed process. (b) Loschmidt echo η in quantum dynamics, which is the fidelity between two states, $e^{-iH\tau}|\Psi(0)\rangle$ and $e^{-iH^*\tau}|\Psi(0)\rangle$ at $t = \tau$. These states are obtained through forward time evolution induced by H and H^* , respectively. (c) An interpretation of the Loschmidt echo η as the fidelity between two states, $|\Psi(0)\rangle$ and $e^{iH^*\tau}e^{-iH\tau}|\Psi(0)\rangle$, at $t = 0$. The latter state is obtained through forward time evolution by H and the subsequent reversed time evolution by H^* .

$\sum_{m=0}^M V_m \rho_S(t) V_m^\dagger$, where

$$V_0 \equiv \mathbb{I}_S - i\Delta t H_S - \frac{1}{2}\Delta t \sum_{m=1}^M L_m^\dagger L_m, \quad (3)$$

$$V_m \equiv \sqrt{\Delta t} L_m \quad (1 \leq m \leq M), \quad (4)$$

where \mathbb{I}_S denotes the identity operator in S (the other identity operators are defined in the same way). V_0 corresponds to no jump and V_m ($1 \leq m \leq M$) to the m th jump within the interval $[t, t + \Delta t]$. V_m ($0 \leq m \leq M$) satisfies the completeness relation $\sum_{m=0}^M V_m^\dagger V_m = \mathbb{I}_S$. V_m defined in Eqs. (3) and (4) are not the only operators that are consistent with Eq. (2). There are infinitely many operators that can induce the same time evolution.

Using the input-output formalism [35–38], employed in studying TURs in a quantum domain [28, 30], we describe the time evolution generated by the Kraus operators (3) and (4) as interactions between the principal system S and the environment E [Fig. 2(a)]. Let $t = 0$ and $t = \tau$ be the initial and final time of time evolution, respectively. We discretize the time interval $[0, \tau]$ by dividing it into N intervals, where N is a sufficiently large number, and we define $\Delta t \equiv \tau/N$ and $t_k \equiv \Delta t k$ ($t_0 = 0$ and $t_N = \tau$). Here, the orthonormal basis of E is assumed to be $|m_{N-1}, \dots, m_1, m_0\rangle$ ($m_k \in \{0, 1, \dots, M-1, M\}$), where a subspace $|m_k\rangle$ interacts with S through a unitary operator U_{t_k} during an interval $[t_k, t_{k+1}]$ [Fig. 2(a)]. When the initial states of S and E are $|\psi_S\rangle$ and $|0_{N-1}, \dots, 0_1, 0_0\rangle$, respectively, the composite state at $t = \tau$ is

$$|\Psi(\tau)\rangle = U_{t_{N-1}} \cdots U_{t_0} |\psi_S\rangle \otimes |0_{N-1}, \dots, 0_0\rangle = \sum_{\mathbf{m}} V_{m_{N-1}} \cdots V_{m_0} |\psi_S\rangle \otimes |m_{N-1}, \dots, m_0\rangle, \quad (5)$$

where $V_{m_k} = \langle m_k | U_{t_k} | 0_k \rangle$ can be viewed as an action on S associated with the transition from $|0_k\rangle$ to $|m_k\rangle$ in E .

Calculating $\text{Tr}_E[|\Psi(\tau)\rangle \langle \Psi(\tau)|]$ for $\Delta t \rightarrow 0$, we recover the original Lindblad equation of Eq. (2).

Continuous measurement [39, 40] of the principal system through the environment corresponds to environmental measurement at the final time [Fig. 2(a)]. When we measure the environment at $t = \tau$ through projectors $|\mathbf{m}\rangle \langle \mathbf{m}|$ with $\mathbf{m} \equiv [m_{N-1}, \dots, m_1, m_0]$, we obtain a realization of \mathbf{m} , and the principal system is projected to $V_{m_{N-1}} \cdots V_{m_0} |\psi_S\rangle$ (note that this is unnormalized). Thus, \mathbf{m} consists of a measurement record of continuous measurement. Since the evolution of $V_{m_{N-1}} \cdots V_{m_0} |\psi_S\rangle$ is stochastic depending on the measurement record, it is referred to as a *quantum trajectory*, which can be described by the stochastic Schrödinger equation [41]. In classical TURs, we consider a counting observable that counts and weights transitions in the stochastic trajectory. The counting observable in the classical stochastic thermodynamics is $\sum_{j \neq i} C_{ji} \mathcal{N}_{ji}$, where \mathcal{N}_{ji} is the number of transitions from i th to j th state in the entire time interval, and $C_{ji} \in \mathbb{R}$ is its weight. The *current* observable additionally assumes anti-symmetry $C_{ji} = -C_{ij}$. Similarly, in a quantum Markov process, we count the number of jumps in a quantum trajectory. Let us consider a measurement (Hermitian) operator \mathcal{C} on E , which admits the following eigendecomposition:

$$\mathcal{C} = \sum_{\mathbf{m}} g(\mathbf{m}) |\mathbf{m}\rangle \langle \mathbf{m}| = \sum_c c \Upsilon(c), \quad (6)$$

where $\Upsilon(c) \equiv \sum_{\mathbf{m}: g(\mathbf{m})=c} |\mathbf{m}\rangle \langle \mathbf{m}|$. A set $\{\Upsilon(c)\}_c$ consists of a projection-valued measure (PVM). We assume that $g(\mathbf{m})$ in Eq. (6) counts and weights jumps in a measurement record \mathbf{m} , which defines a counting observable in quantum Markov processes. We use $g(\mathbf{m}) = \sum_{k=0}^{N-1} C_{m_k}$, where $C \equiv [C_0, C_1, \dots, C_M] = [0, a_1, \dots, a_M]$ ($a_i \in \mathbb{R}$) is a projection vector specifying the weight of each jump. For instance, for $M = 1$ (i.e., a single jump operator), an example of the measurement record would be $\mathbf{m} = [0, 0, 1, 0, \dots, 0, 1, 0, 0]$, where 1s denote the detection of jumps. When $C = [0, 1]$, $g(\mathbf{m})$ sim-

ply counts the number of jumps in \mathbf{m} . Then, $\Upsilon(c)$ corresponds to a set of measurement records \mathbf{m} that produces a particular observable value $c = g(\mathbf{m})$. Let $\mathbb{P}(c) \equiv \langle \Psi(\tau) | \mathbb{I}_S \otimes \Upsilon(c) | \Psi(\tau) \rangle$, which is the probability distribution of counting observable ($\mathbb{P}_*(c)$ is defined in the same way for the perturbed dynamics $|\Psi_*(\tau)\rangle$). Figure 2(b) shows an example of $\mathbb{P}(c)$ and $\mathbb{P}_*(c)$. $\mathbb{P}(c)$ and $\mathbb{P}_*(c)$ in Fig. 2(b) denote the probability distributions for the number of jump events within $[0, \tau]$ for the original and perturbed dynamics, respectively. The mean and variance of the counting observable are calculated by $\langle \mathcal{C} \rangle = \sum_c c \mathbb{P}(c)$ and $\|\mathcal{C}\|^2 = \sum_c c^2 \mathbb{P}(c) - \langle \mathcal{C} \rangle^2$.

The Loschmidt echo considers the fidelity between the original $|\Psi\rangle$ and the perturbed state $|\Psi_*\rangle$ [Eq. (1)]. Let $H_{*,S}$ and $L_{*,m}$ ($1 \leq m \leq M$) be perturbed Hamiltonian and jump operator in Eqs. (3) and (4). Then, we define the Kraus operators of the perturbed dynamics $V_{*,m}$ by Eqs. (3) and (4), where H_S and L_m should be replaced with $H_{*,S}$ and $L_{*,m}$, respectively. Similar to Eq. (5), the composite state of the perturbed dynamics at $t = \tau$ is given by

$$|\Psi_*(\tau)\rangle = \sum_m V_{*,m_{N-1}} \cdots V_{*,m_0} |\psi_S\rangle \otimes |m_{N-1}, \dots, m_0\rangle. \quad (7)$$

Calculating the Loschmidt echo $|\langle \Psi_* | \Psi \rangle|^2$ for Eqs. (5) and (7) is not an easy task since the composite state $[(\Psi(\tau)) \text{ or } |\Psi_*(\tau)\rangle]$, consisting of the principal system and environment, is inaccessible in general. For continuous measurement, the Loschmidt echo can be calculated explicitly after Refs. [36, 43]. Note that $\langle \Psi_*(t) | \Psi(t) \rangle = \text{Tr}_{SE} [|\Psi(t)\rangle \langle \Psi_*(t)|] = \text{Tr}_S [\phi(t)]$ where $\phi(t) \equiv \text{Tr}_E [|\Psi(t)\rangle \langle \Psi_*(t)|]$. Thus, using Eqs. (5) and (7), ϕ satisfies a two-sided Lindblad equation [36, 43]:

$$\begin{aligned} \dot{\phi} = \mathcal{K}\phi &\equiv -iH_S\phi + i\phi H_{*,S} + \sum_m L_m \phi L_{*,m}^\dagger \\ &- \frac{1}{2} \sum_m [L_m^\dagger L_m \phi + \phi L_{*,m}^\dagger L_{*,m}], \end{aligned} \quad (8)$$

where \mathcal{K} is a super-operator. Note that ϕ does not preserve the trace, i.e., $\text{Tr}_S[\phi(t)] \neq 1$ in general. By solving the two-sided Lindblad equation, we obtain $\phi(\tau) = e^{\mathcal{K}\tau} \rho_S(0)$, where $\rho_S(0) = |\psi_S\rangle \langle \psi_S|$ is the initial density operator of the Lindblad dynamics [44]. The Loschmidt echo η is expressed by $\eta = |\text{Tr}_S [e^{\mathcal{K}\tau} \rho_S(0)]|^2$. Importantly, η can be specified by quantities of S alone (H_S , L_m , $H_{*,S}$, and $L_{*,m}$). We do not require information about E , which is inaccessible in general. The above calculations assumed an initially pure state; however, a generalization to an initially mixed state case is straightforward [41].

Next, we relate the precision of the counting observable \mathcal{C} with the Loschmidt echo η . Let \mathcal{F} be an arbitrary Hermitian measurement operator on $|\Psi\rangle$ and $|\Psi_*\rangle$. \mathcal{F} admits the eigendecomposition $\mathcal{F} = \sum_z f(z) \Lambda(z)$, where

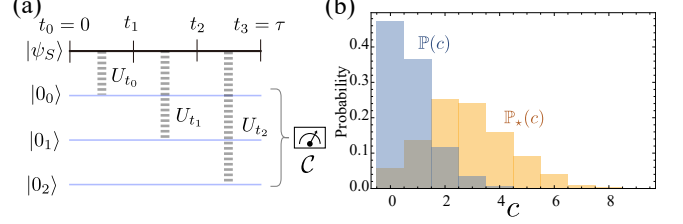


FIG. 2. Illustration of continuous measurement. (a) Illustration of continuous measurement model for $N = 3$. The initial states of S and E are $|\psi_S\rangle$ and $|0_2, 0_1, 0_0\rangle$, respectively. The environment subspace $|0_k\rangle$ interacts with S via a unitary operator U_{t_k} during an interval $[t_k, t_{k+1}]$. Finally, at $t = \tau$, E is measured by \mathcal{C} . (b) Probability distributions of a counting observable \mathcal{C} . $\mathbb{P}(c)$ and $\mathbb{P}_*(c)$ represent the probability distributions for the original and perturbed dynamics, respectively. In this example, these distributions are calculated for a two-level atom driven by a laser field, and the counting observable is the number of jump events ([41] for details).

$f(z)$ and $\Lambda(z)$ represent an eigenvalue and its corresponding projector, respectively. Using the projector $\Lambda(z)$, we obtain that the fidelity is bounded from above by

$$\begin{aligned} |\langle \Psi_* | \Psi \rangle| &\leq \sum_z |\langle \Psi_* | \Lambda(z) | \Psi \rangle| \leq \sum_z \sqrt{P(z)} \sqrt{P_*(z)} \\ &= 1 - \mathcal{H}^2(P, P_*). \end{aligned} \quad (9)$$

where $P(z) \equiv \langle \Psi | \Lambda(z) | \Psi \rangle$, $P_*(z) \equiv \langle \Psi_* | \Lambda(z) | \Psi_* \rangle$, and $\mathcal{H}^2(\bullet, \bullet)$ is the Hellinger distance. Given two distributions $P(z)$ and $Q(z)$, we define the Hellinger distance as follows:

$$\mathcal{H}^2(P, Q) = \frac{1}{2} \sum_z \left(\sqrt{P(z)} - \sqrt{Q(z)} \right)^2, \quad (10)$$

where $0 \leq \mathcal{H}^2(P, Q) \leq 1$. The Hellinger distance has a lower bound, given the mean and variance [45–47]. We use a tighter lower bound recently derived in Ref. [47] (see also Ref. [48]):

$$\mathcal{H}^2(P, Q) \geq 1 - \left[\left(\frac{\langle f \rangle_P - \langle f \rangle_Q}{\|\mathcal{F}\|_P + \|\mathcal{F}\|_Q} \right)^2 + 1 \right]^{-\frac{1}{2}}, \quad (11)$$

where $\langle f \rangle_P = \sum_z f(z)P(z)$ and $\|\mathcal{F}\|_P = \sqrt{\langle \mathcal{F}^2 \rangle_P - \langle \mathcal{F} \rangle_P^2}$ represent the mean and standard deviation, respectively. Substituting Eq. (11) into Eq. (9), we obtain

$$\left(\frac{\|\mathcal{F}\| + \|\mathcal{F}\|_*}{\langle \mathcal{F} \rangle - \langle \mathcal{F} \rangle_*} \right)^2 \geq \frac{1}{\eta^{-1} - 1}, \quad (12)$$

where $\langle \mathcal{F} \rangle \equiv \langle \Psi | \mathcal{F} | \Psi \rangle$ and $\|\mathcal{F}\| \equiv \sqrt{\langle \mathcal{F}^2 \rangle - \langle \mathcal{F} \rangle^2}$ (quantities with a subscript $*$ should be evaluated for $|\Psi_*\rangle$ instead of $|\Psi\rangle$). Note that a similar relation, which is looser than Eq. (12), was derived in Ref. [49]. By taking

$\mathcal{F} = \mathbb{I}_S \otimes \mathcal{C}$ in Eq. (12), where \mathcal{C} is the counting observable defined in Eq. (6), we obtain

$$\left(\frac{\llbracket \mathcal{C} \rrbracket + \llbracket \mathcal{C} \rrbracket_\star}{\langle \mathcal{C} \rangle - \langle \mathcal{C} \rangle_\star} \right)^2 \geq \frac{1}{|\text{Tr}_S [e^{\kappa\tau} \rho_S(0)]|^{-2} - 1}, \quad (13)$$

which is the main result of this Letter. The left-hand side of Eq. (13) concerns the counting observable \mathcal{C} , while the right-hand side can be calculated through $H_S, H_{\star,S}, L_m, L_{\star,m}$ [Eq. (8)], and $\rho_S(0)$. Equation (13) shows that the precision of counting observables is improved when the extent of irreversibility increases, which qualitatively agrees with the classical TURs [1, 2]. Classical TURs have a lower bound based on the entropy production that characterizes the irreversibility of classical Markov processes. Equation (13) is reminiscent of a hysteretic TUR [50], which considers an observable of two different processes. Similarly, Eq. (13) includes the mean and variance of two dynamics, the original and perturbed dynamics. The Kraus operator V_m in Eqs. (3) and (4) are not unique and depend on the continuous measurement. We can show that Eq. (13) still holds for any continuous measurement (any unravelling) [41].

For a specific case, Eq. (13) covers classical stochastic processes. Consider a classical Markov chain with N_S states. Such classical states can be represented quantum mechanically by an orthonormal basis $|b_1\rangle, |b_2\rangle, \dots, |b_{N_S}\rangle$. Let γ_{ji} be a transition rate from $|b_i\rangle$ to $|b_j\rangle$ for the original dynamics ($\gamma_{\star,ji}$ is defined in the same way for the perturbed dynamics) and $p_i(t)$ be the probability of being i th state at time t . In a classical limit, Eq. (8) reduces to

$$\dot{\varphi}_i = \sum_{j(\neq i)} \sqrt{\gamma_{ij} \gamma_{\star,ij}} \varphi_j - \frac{1}{2} \varphi_i \sum_{j(\neq i)} (\gamma_{ji} + \gamma_{\star,ji}), \quad (14)$$

where $\varphi_i \equiv \langle b_i | \phi | b_i \rangle$ and $\varphi_i(0) = p_i(0)$.

We consider a specific case of the empty perturbed dynamics in Eq. (13), i.e., $H_{\star,S} = 0$ and $L_{\star,m} = 0$ for all m . Here, the composite state of the perturbed dynamics at $t = \tau$ is $|\Psi_\star(\tau)\rangle = |\psi_S\rangle \otimes |0_{N-1}, \dots, 0_0\rangle$, which is unchanged from the initial state. In this case, the Loschmidt echo is $\eta = |\langle \Psi(0) | \Psi(\tau) \rangle|^2$. Since \mathcal{C} counts the number of jumps in the measurement record \mathbf{m} , it should vanish at the initial state since there is no jump at $t = 0$. Thus, $\langle \mathcal{C} \rangle_\star = 0$ and $\llbracket \mathcal{C} \rrbracket_\star = 0$ for the empty dynamics. Equation (13) becomes

$$\frac{\llbracket \mathcal{C} \rrbracket^2}{\langle \mathcal{C} \rangle^2} \geq \frac{1}{\left| \text{Tr}_S \left[e^{\left(-iH_S - \frac{1}{2} \sum_m L_m^\dagger L_m \right) \tau} \rho_S(0) \right] \right|^{-2} - 1}. \quad (15)$$

The bound of Eq. (15) is similar to that obtained in Ref. [30]. Note that there is no definite magnitude relation between Eq. (15) and that in Ref. [30]. In the short time limit $\tau \rightarrow 0$, we obtain $\llbracket \mathcal{C} \rrbracket^2 / \langle \mathcal{C} \rangle^2 \geq 1 / [\text{Tr}_S [\sum_m L_m^\dagger L_m \rho_S(0)] \tau]$, where the denominator corresponds to the dynamical activity [51] in classical

Markov processes. Although Eq. (13) does not depend on continuous measurement, Eq. (15) does not hold for arbitrary continuous measurement in general [41]. Using the classical assumption used in deriving Eq. (14), we can obtain a classical limit of Eq. (15) as follows:

$$\frac{\llbracket \mathcal{C} \rrbracket^2}{\langle \mathcal{C} \rangle^2} \geq \frac{1}{\left(\sum_i p_i(0) \sqrt{e^{-\sum_{j(\neq i)} \gamma_{ji} \tau}} \right)^{-2} - 1}. \quad (16)$$

The expression inside the square root in Eq. (16) corresponds to the probability of no jump within $[0, \tau]$ starting from $|b_i\rangle$. The denominator of Eq. (16) is an experimentally measurable quantity.

The left-hand side of Eq. (13) becomes smaller when the “distance” between the two distributions $\mathbb{P}(c)$ and $\mathbb{P}_\star(c)$ is larger. Thus, Eq. (13) can be viewed as a relation between the “distance” and Loschmidt echo. Here, we show that an upper bound for the distance between $\mathbb{P}(c)$ and $\mathbb{P}_\star(c)$ can be directly obtained using the Loschmidt echo η . Let us consider a trace distance $\mathcal{T}(\rho, \varsigma) \equiv \frac{1}{2} \text{Tr} \left[\sqrt{(\rho - \varsigma)^2} \right]$ [52], which ranges within $[0, 1]$. When ρ and ς are pure states given by $|\psi\rangle$ and $|\xi\rangle$, respectively, the trace distance becomes $\mathcal{T}(|\psi\rangle, |\xi\rangle) = \sqrt{1 - |\langle \psi | \xi \rangle|^2}$. Let \mathcal{M} be a positive operator-valued measure (POVM) and $\mathcal{M}(\rho)$ be probability distribution obtained by applying \mathcal{M} to a density operator ρ . The trace distance satisfies

$$\mathcal{T}(\rho, \varsigma) \geq \delta(\mathcal{M}(\rho), \mathcal{M}(\varsigma)), \quad (17)$$

where $\delta(P, Q) \equiv \frac{1}{2} \sum_m |P(m) - Q(m)|$ is a total variation distance, given two probability distributions $P(m)$ and $Q(m)$. The total variation distance quantifies the similarity between two probability distributions and ranges within $[0, 1]$. Let us consider $\rho = |\Psi(\tau)\rangle \langle \Psi(\tau)|$, $\varsigma = |\Psi_\star(\tau)\rangle \langle \Psi_\star(\tau)|$, and $\mathcal{M} = \{\mathbb{I}_S \otimes \Upsilon(c)\}_c$ in Eq. (17), in which $\mathcal{M}(\rho)$ and $\mathcal{M}(\varsigma)$ give $\mathbb{P}(c)$ and $\mathbb{P}_\star(c)$, respectively. Then, we determine an upper bound for a total variation distance between $\mathbb{P}(c)$ and $\mathbb{P}_\star(c)$, which represent probability distributions of the counting observable \mathcal{C} in the original and perturbed dynamics, as follows:

$$\delta(\mathbb{P}, \mathbb{P}_\star) \leq \sqrt{1 - |\text{Tr} [e^{\kappa\tau} \rho_S(0)]|^2}, \quad (18)$$

which is the second main result of this Letter. In Eq. (18), the left-hand side is characterized by the distribution on counting observable, while the right-hand side is calculated through $H_S, H_{\star,S}, L_m, L_{\star,m}$ [Eq. (8)], and $\rho_S(0)$. Equation (18) states that probability distributions of counting observable in two dynamics become closer with respect to the total variation distance when the Loschmidt echo of the dynamics is larger. As in Eq. (13), Eq. (18) holds for any continuous measurement since POVM \mathcal{M} in Eq. (17) can be arbitrary. Besides, Eq. (18) holds for classical Markov processes. However, a classical analog of Eq. (18) has not been reported yet.

We perform simulation analysis for Eqs. (13) and (18) and numerically verify the bounds.

Conclusion.—In this Letter, we obtained a relation between the Loschmidt echo and precision of continuous measurement in quantum Markov processes, which can be viewed as a quantum generalization of classical TURs. We obtained an upper bound for the total variation distance between two counting observable distributions using the Loschmidt echo. Since relations derived in this Letter utilized the advantage of general quantum bounds, which hold for general Hermitian observables, we can obtain other thermodynamic relations for the counting observable through our approach.

This work was supported by the Ministry of Education, Culture, Sports, Science and Technology (MEXT) KAKENHI Grant No. JP19K12153.

* hasegawa@biom.t.u-tokyo.ac.jp

- [1] A. C. Barato and U. Seifert, Thermodynamic uncertainty relation for biomolecular processes, *Phys. Rev. Lett.* **114**, 158101 (2015).
- [2] T. R. Gingrich, J. M. Horowitz, N. Perunov, and J. L. England, Dissipation bounds all steady-state current fluctuations, *Phys. Rev. Lett.* **116**, 120601 (2016).
- [3] P. Pietzonka, A. C. Barato, and U. Seifert, Universal bounds on current fluctuations, *Phys. Rev. E* **93**, 052145 (2016).
- [4] J. M. Horowitz and T. R. Gingrich, Proof of the finite-time thermodynamic uncertainty relation for steady-state currents, *Phys. Rev. E* **96**, 020103 (2017).
- [5] S. Pigolotti, I. Neri, E. Roldán, and F. Jülicher, Generic properties of stochastic entropy production, *Phys. Rev. Lett.* **119**, 140604 (2017).
- [6] J. P. Garrahan, Simple bounds on fluctuations and uncertainty relations for first-passage times of counting observables, *Phys. Rev. E* **95**, 032134 (2017).
- [7] A. Dechant and S.-i. Sasa, Current fluctuations and transport efficiency for general Langevin systems, *J. Stat. Mech: Theory Exp.* **2018**, 063209 (2018).
- [8] A. C. Barato, R. Chetrite, A. Faggionato, and D. Gabrielli, Bounds on current fluctuations in periodically driven systems, *New J. Phys.* **20** (2018).
- [9] I. D. Terlizzi and M. Baiesi, Kinetic uncertainty relation, *J. Phys. A: Math. Theor.* **52**, 02LT03 (2019).
- [10] Y. Hasegawa and T. Van Vu, Uncertainty relations in stochastic processes: An information inequality approach, *Phys. Rev. E* **99**, 062126 (2019).
- [11] Y. Hasegawa and T. Van Vu, Fluctuation theorem uncertainty relation, *Phys. Rev. Lett.* **123**, 110602 (2019).
- [12] T. Van Vu and Y. Hasegawa, Uncertainty relations for underdamped Langevin dynamics, *Phys. Rev. E* **100**, 032130 (2019).
- [13] T. Van Vu and Y. Hasegawa, Thermodynamic uncertainty relations under arbitrary control protocols, *Phys. Rev. Research* **2**, 013060 (2020).
- [14] A. Dechant and S.-i. Sasa, Fluctuation-response inequality out of equilibrium, *Proc. Natl. Acad. Sci. U.S.A.* **117**, 6430 (2020).
- [15] V. T. Vo, T. Van Vu, and Y. Hasegawa, Unified approach to classical speed limit and thermodynamic uncertainty relation, *Phys. Rev. E* **102**, 062132 (2020).
- [16] T. Koyuk and U. Seifert, Thermodynamic uncertainty relation for time-dependent driving, *Phys. Rev. Lett.* **125**, 260604 (2020).
- [17] A. Dechant and S. ichi Sasa, Continuous time-reversal and equality in the thermodynamic uncertainty relation, *arXiv:2010.14769* (2020).
- [18] J. M. Horowitz and T. R. Gingrich, Thermodynamic uncertainty relations constrain non-equilibrium fluctuations, *Nat. Phys.* (2019).
- [19] A. Peres, Stability of quantum motion in chaotic and regular systems, *Phys. Rev. A* **30**, 1610 (1984).
- [20] T. Gorin, T. Prosen, T. H. Seligman, and M. Žnidarič, Dynamics of Loschmidt echoes and fidelity decay, *Phys. Rep.* **435**, 33 (2006).
- [21] A. Goussev, R. A. Jalabert, H. M. Pastawski, and D. Wisniacki, Loschmidt echo, *arXiv:1206.6348* (2012).
- [22] P. Erker, M. T. Mitchison, R. Silva, M. P. Woods, N. Brunner, and M. Huber, Autonomous quantum clocks: Does thermodynamics limit our ability to measure time?, *Phys. Rev. X* **7**, 031022 (2017).
- [23] K. Brandner, T. Hanazato, and K. Saito, Thermodynamic bounds on precision in ballistic multiterminal transport, *Phys. Rev. Lett.* **120**, 090601 (2018).
- [24] F. Carollo, R. L. Jack, and J. P. Garrahan, Unraveling the large deviation statistics of Markovian open quantum systems, *Phys. Rev. Lett.* **122**, 130605 (2019).
- [25] J. Liu and D. Segal, Thermodynamic uncertainty relation in quantum thermoelectric junctions, *Phys. Rev. E* **99**, 062141 (2019).
- [26] G. Guarneri, G. T. Landi, S. R. Clark, and J. Goold, Thermodynamics of precision in quantum nonequilibrium steady states, *Phys. Rev. Research* **1**, 033021 (2019).
- [27] S. Saryal, H. M. Friedman, D. Segal, and B. K. Agarwalla, Thermodynamic uncertainty relation in thermal transport, *Phys. Rev. E* **100**, 042101 (2019).
- [28] Y. Hasegawa, Quantum thermodynamic uncertainty relation for continuous measurement, *Phys. Rev. Lett.* **125**, 050601 (2020).
- [29] H. M. Friedman, B. K. Agarwalla, O. Shein-Lumbroso, O. Tal, and D. Segal, Thermodynamic uncertainty relation in atomic-scale quantum conductors, *Phys. Rev. B* **101**, 195423 (2020).
- [30] Y. Hasegawa, Thermodynamic uncertainty relation for general open quantum systems, *Phys. Rev. Lett.* **126**, 010602 (2021).
- [31] M. F. Sacchi, Thermodynamic uncertainty relations for bosonic Otto engines, *Phys. Rev. E* **103**, 012111 (2021).
- [32] A. A. S. Kalaee, A. Wacker, and P. P. Potts, Violating the thermodynamic uncertainty relation in the three-level maser, *arXiv:2103.07791* (2021).
- [33] G. Lindblad, On the generators of quantum dynamical semigroups, *Commun. Math. Phys.* **48**, 119 (1976).
- [34] H.-P. Breuer and F. Petruccione, *The theory of open quantum systems* (Oxford university press, 2002).
- [35] M. Guță, Fisher information and asymptotic normality in system identification for quantum Markov chains, *Phys. Rev. A* **83**, 062324 (2011).
- [36] S. Gammelmark and K. Mølmer, Fisher information and the quantum Cramér-Rao sensitivity limit of continuous measurements, *Phys. Rev. Lett.* **112**, 170401 (2014).

[37] K. Macieszczak, M. Gută, I. Lesanovsky, and J. P. Garrahan, Dynamical phase transitions as a resource for quantum enhanced metrology, *Phys. Rev. A* **93**, 022103 (2016).

[38] J. A. Gross, C. M. Caves, G. J. Milburn, and J. Combes, Qubit models of weak continuous measurements: Markovian conditional and open-system dynamics, *Quantum Sci. Technol.* **3**, 024005 (2018).

[39] H. M. Wiseman, Quantum trajectories and quantum measurement theory, *J. Eur. Opt. Soc. Part B* **8**, 205 (1996).

[40] C. Elouard and M. H. Mohammady, Work, heat and entropy production along quantum trajectories, in *Thermodynamics in the Quantum Regime: Fundamental Aspects and New Directions*, edited by F. Binder, L. A. Correa, C. Gogolin, J. Anders, and G. Adesso (Springer International Publishing, Cham, 2018) pp. 363–393.

[41] See Supplemental Material for details of calculations, which includes Ref. [42].

[42] G. T. Landi, *Quantum Information and Quantum Noise*, Tech. Rep. (University of São Paulo, <http://www.fmt.if.usp.br/~gtlandi/quantum-information-and.html>, 2018).

[43] K. Mølmer, Hypothesis testing with open quantum systems, *Phys. Rev. Lett.* **114**, 040401 (2015).

[44] Since \mathcal{K} is a super-operator, evaluating $e^{\mathcal{K}\tau}$ requires the calculation in the Liouville space [41].

[45] M. Dashti and A. M. Stuart, The Bayesian approach to inverse problems, in *Handbook of Uncertainty Quantification*, edited by R. Ghanem, D. Higdon, and H. Owhadi (2017) pp. 311–428.

[46] M. A. Katsoulakis, L. Rey-Bellet, and J. Wang, Scalable information inequalities for uncertainty quantification, *J. Comput. Phys.* **336**, 513 (2017).

[47] T. Nishiyama, A tight lower bound for the Hellinger distance with given means and variances, [arXiv:2010.13548](https://arxiv.org/abs/2010.13548) (2020).

[48] T. Nishiyama and I. Sason, On relations between the relative entropy and χ^2 -divergence, generalizations and applications, *Entropy* **22**, 563 (2020).

[49] A. S. Holevo, A generalization of the Rao–Cramér inequality, *Teoriya Veroyatnostei i ee Primeneniya* **18**, 371 (1973).

[50] K. Proesmans and J. M. Horowitz, Hysteretic thermodynamic uncertainty relation for systems with broken time-reversal symmetry, *J. Stat. Mech: Theory Exp.* **2019**, 054005 (2019).

[51] C. Maes, Frenesy: Time-symmetric dynamical activity in nonequilibria, *Phys. Rep.* **850**, 1 (2020).

[52] M. A. Nielsen and I. L. Chuang, *Quantum Computation and Quantum Information* (Cambridge University Press, New York, NY, USA, 2011).

Supplementary Material for “Irreversibility, Loschmidt Echo, and Thermodynamic Uncertainty Relation”

Yoshihiko Hasegawa*

*Department of Information and Communication Engineering,
Graduate School of Information Science and Technology,
The University of Tokyo, Tokyo 113-8656, Japan*

This supplementary material describes the calculations introduced in the main text. Equation and figure numbers are prefixed with S (e.g., Eq. (S1) or Fig. S1). Numbers without this prefix (e.g., Eq. (1) or Fig. 1) refer to items in the main text.

S1. LIOUVILLE SPACE REPRESENTATION

The Lindblad equation describes the time evolution of a density operator ρ_S in Hilbert space. It can be equivalently described in Liouville space. Here, we introduce the Liouville space representation according to Ref. [1]. Given an orthonormal basis $|i\rangle$ in S , the density operator is

$$\rho_S = \sum_{i,j} \varrho_{ij} |i\rangle \langle j|. \quad (\text{S1})$$

We introduce a vectorization of ρ_S by

$$\text{vec}(\rho_S) \equiv \sum_{i,j} \varrho_{ij} |j\rangle \otimes |i\rangle. \quad (\text{S2})$$

Note that $\text{vec}(\rho)$ belongs to a Liouville space. Using the vectorization, we can express the two-sided Lindblad equation in a Liouville space. The two-sided Lindblad equation is given by [see Eq. (8) in the main text]

$$\dot{\phi} = \mathcal{K}\phi \equiv -iH_S\phi + i\phi H_{\star,S} + \sum_m L_m\phi L_{\star,m}^\dagger - \frac{1}{2} \sum_m [L_m^\dagger L_m\phi + \phi L_{\star,m}^\dagger L_{\star,m}], \quad (\text{S3})$$

where H_S is a Hamiltonian and L_m is a jump operator of the original dynamics, and $H_{\star,S}$ and $L_{\star,S}$ represent the Hamiltonian and jump operator in perturbed dynamics. We assume that there are M jump operators L_m . The Liouville representation of Eq. (S3) is given as follows:

$$\frac{d}{dt} \text{vec}(\phi) = \hat{\mathcal{K}} \text{vec}(\phi), \quad (\text{S4})$$

where $\hat{\mathcal{K}}$ is defined by

$$\hat{\mathcal{K}} \equiv -i [\mathbb{I}_S \otimes H_S - H_{\star,S}^\top \otimes \mathbb{I}_S] + \sum_m \left[L_{\star,m}^* \otimes L_m - \frac{1}{2} \mathbb{I}_S \otimes L_m^\dagger L_m - \frac{1}{2} (L_{\star,m}^\dagger L_{\star,m})^\top \otimes \mathbb{I}_S \right], \quad (\text{S5})$$

where $*$ denotes the complex conjugate and \top denotes the transpose. Since Eq. (S4) is a simple linear differential equation, its solution is given by

$$\text{vec}(\phi(\tau)) = e^{\hat{\mathcal{K}}\tau} \text{vec}(\rho_S(0)), \quad (\text{S6})$$

which is abbreviated as $\phi(\tau) = e^{\mathcal{K}\tau} \rho_S(0)$ in the main text.

In the main text, we consider a case where the perturbed dynamics is empty, i.e., $H_{\star,S} = 0$ and $L_{\star,m} = 0$ for all m . Here, Eq. (S3) becomes

$$\dot{\phi} = \left[-iH_S - \frac{1}{2} \sum_m L_m^\dagger L_m \right] \phi, \quad (\text{S7})$$

which is a simple linear differential equation. Thus, the solution of Eq. (S7) can be represented in a Hilbert space as follows:

$$\phi(\tau) = e^{[-iH_S - \frac{1}{2} \sum_m L_m^\dagger L_m]\tau} \rho_S(0). \quad (\text{S8})$$

* hasegawa@biom.t.u-tokyo.ac.jp

S2. MIXED STATE CASE

In the main text, we consider a two-sided Lindblad equation for initially pure states. In this section, we consider a two-sided Lindblad equation for an initially mixed state.

Let ρ_S be the initial mixed state in S . We consider an ancilla A that purifies ρ_S . Let $|\tilde{\psi}_{SA}\rangle$ in $S+A$ be a purification of ρ_S :

$$\rho_S = \text{Tr}_A \left[|\tilde{\psi}_{SA}\rangle \langle \tilde{\psi}_{SA}| \right]. \quad (\text{S9})$$

We want to define the time evolution on a pure state in $S+A$. We define the following Kraus operators on $S+A$:

$$\tilde{V}_m \equiv V_m \otimes \mathbb{I}_A \quad (0 \leq m \leq M), \quad (\text{S10})$$

where V_m is defined in Eqs. (3) and (4). By applying \tilde{V}_m to the purified state $|\tilde{\psi}_{SA}\rangle$ and tracing the ancilla A , we obtain

$$\begin{aligned} \text{Tr}_A \left[\sum_{m=0}^M \tilde{V}_m |\tilde{\psi}_{SA}\rangle \langle \tilde{\psi}_{SA}| \tilde{V}_m^\dagger \right] &= \text{Tr}_A \left[\sum_{m=0}^M (V_m \otimes \mathbb{I}_A) |\tilde{\psi}_{SA}\rangle \langle \tilde{\psi}_{SA}| (V_m^\dagger \otimes \mathbb{I}_A) \right] \\ &= \sum_{m=0}^M V_m \text{Tr}_A \left[|\tilde{\psi}_{SA}\rangle \langle \tilde{\psi}_{SA}| \right] V_m^\dagger \\ &= \sum_{m=0}^M V_m \rho_S V_m^\dagger, \end{aligned} \quad (\text{S11})$$

indicating that \tilde{V}_m induces the consistent time evolution for ρ_S in S . Using \tilde{V}_m defined in Eq. (S10), similar to Eq. (5), a pure state in $S+A+E$ at $t=\tau$ is represented by

$$|\tilde{\Psi}(\tau)\rangle = \sum_{\mathbf{m}} \tilde{V}_{m_{N-1}} \cdots \tilde{V}_{m_0} |\tilde{\psi}_{SA}\rangle \otimes |m_{N-1}, \dots, m_0\rangle, \quad (\text{S12})$$

As stated in the main text, $\mathbf{m} = [m_{N-1}, \dots, m_1, m_0]$ is a measurement record of the observation of the environment E with projector $|\mathbf{m}\rangle \langle \mathbf{m}|$. For $|\tilde{\Psi}(\tau)\rangle$, we calculate the probability of obtaining \mathbf{m} :

$$\begin{aligned} P(m_{N-1}, \dots, m_0) &= \langle \tilde{\Psi}(\tau) | \mathbb{I}_S \otimes \mathbb{I}_S \otimes |m_{N-1}, \dots, m_0\rangle \langle m_{N-1}, \dots, m_0 | \tilde{\Psi}(\tau) \rangle \\ &= \langle \tilde{\psi}_{SA} | \tilde{V}_{m_0}^\dagger \cdots \tilde{V}_{m_{N-1}}^\dagger \tilde{V}_{m_{N-1}} \cdots \tilde{V}_{m_0} | \tilde{\psi}_{SA} \rangle \\ &= \text{Tr}_{SA} \left[\tilde{V}_{m_{N-1}} \cdots \tilde{V}_{m_0} |\tilde{\psi}_{SA}\rangle \langle \tilde{\psi}_{SA}| \tilde{V}_{m_0}^\dagger \cdots \tilde{V}_{m_{N-1}}^\dagger \right] \\ &= \text{Tr}_S \left[V_{m_{N-1}} \cdots V_{m_0} \text{Tr}_A \left[|\tilde{\psi}_{SA}\rangle \langle \tilde{\psi}_{SA}| \right] V_{m_0}^\dagger \cdots V_{m_{N-1}}^\dagger \right] \\ &= \text{Tr}_S \left[V_{m_{N-1}} \cdots V_{m_0} \rho_S V_{m_0}^\dagger \cdots V_{m_{N-1}}^\dagger \right]. \end{aligned} \quad (\text{S13})$$

Thus, statistics of \mathbf{m} obtained by quantum trajectories induced by V_m with an initially mixed state ρ_S are identical to the measurement on $|\tilde{\Psi}(\tau)\rangle$ by $\mathbb{I}_S \otimes \mathbb{I}_A \otimes \mathcal{C}$, where \mathcal{C} is the counting observable defined in Eq. (6).

Similarly, we introduce the Kraus operators $\tilde{V}_{\star,m}$, representing perturbed dynamics:

$$\tilde{V}_{\star,m} \equiv V_{\star,m} \otimes \mathbb{I}_A \quad (0 \leq m \leq M), \quad (\text{S14})$$

where $V_{\star,m}$ is defined in the main text. Similar to Eq. (S12), the pure state of the conjugate dynamics in $S+A+E$ at $t=\tau$ is given as follows:

$$|\tilde{\Psi}_\star(\tau)\rangle = \sum_{\mathbf{m}} \tilde{V}_{\star,m_{N-1}} \cdots \tilde{V}_{\star,m_0} |\tilde{\psi}_{SA}\rangle \otimes |m_{N-1}, \dots, m_0\rangle. \quad (\text{S15})$$

As stated in the main text, we can compute the fidelity as follows:

$$\begin{aligned} \langle \tilde{\Psi}_\star(\tau) | \tilde{\Psi}(\tau) \rangle &= \text{Tr}_{SAE} \left[|\tilde{\Psi}(\tau)\rangle \langle \tilde{\Psi}_\star(\tau)| \right] \\ &= \text{Tr}_{SA} \left[\sum_{\mathbf{m}} \tilde{V}_{m_{N-1}} \cdots \tilde{V}_{m_0} |\tilde{\psi}_{SA}\rangle \langle \tilde{\psi}_{SA}| \tilde{V}_{\star,m_0}^\dagger \cdots \tilde{V}_{\star,m_{N-1}}^\dagger \right] \\ &= \text{Tr}_S \left[\sum_{\mathbf{m}} V_{m_{N-1}} \cdots V_{m_0} \rho_S V_{\star,m_0}^\dagger \cdots V_{\star,m_{N-1}}^\dagger \right]. \end{aligned} \quad (\text{S16})$$

The last line of Eq. (S16) gives a two-sided Lindblad equation with initial state ρ_S .

S3. MEASUREMENT OPERATOR ON THE ENVIRONMENT

The Kraus operator V_m in Eqs. (3) and (4) is not unique. Let \mathcal{B} be a unitary matrix. Any Kraus operator Y_m defined by

$$Y_n = \sum_m \mathcal{B}_{nm} V_m, \quad (\text{S17})$$

gives the same time evolution as V_m , i.e., $\sum_m V_m \rho_S V_m^\dagger = \sum_m Y_m \rho_S Y_m^\dagger$. A different Kraus operator corresponds to a different measurement on the environment E . The basis of the k th environmental subspace is $|m_k\rangle$ where $m_k \in \{0, 1, \dots, M\}$. In this section, we write $|m\rangle$ to express the subspace $|m_k\rangle$. The Kraus operator of Eqs. (3) and (4) corresponds to a measurement with basis $|m\rangle$ for each environmental subspace. Let us consider the basis $|\alpha\rangle$, representing a basis different from $|m\rangle$. $|\alpha\rangle$ is related to $|m\rangle$ through

$$|\alpha\rangle = \sum_m \mathcal{A}_{m\alpha} |m\rangle, \quad (\text{S18})$$

where \mathcal{A} is a unitary operator. A direct calculation shows that the unitary operator \mathcal{A} satisfies $\mathcal{A} = \mathcal{B}^\dagger$, indicating that the unitary freedom in the Kraus operator corresponds to that in the measurement basis. Using $|\alpha\rangle$ and Y_n , Eq. (5) becomes

$$|\Psi(\tau)\rangle = \sum_{\alpha} Y_{\alpha_{N-1}} \cdots Y_{\alpha_0} |\psi_S\rangle \otimes |\alpha_{N-1}, \dots, \alpha_0\rangle, \quad (\text{S19})$$

where $\alpha \equiv [\alpha_{N-1}, \dots, \alpha_1, \alpha_0]$. In the main text, we consider the counting observable defined in Eq. (6) and a measurement on the environment by the projector $|\mathbf{m}\rangle\langle\mathbf{m}|$. Here, we obtain a realization of \mathbf{m} , and the principal system is projected to $V_{m_{N-1}} \cdots V_{m_0} |\psi\rangle$. Similarly, we can employ a different projector $|\alpha\rangle\langle\alpha|$ for the environmental measurement. Using $|\alpha\rangle\langle\alpha|$, we obtain a realization of α , and the principal system is projected to $Y_{\alpha_{N-1}} \cdots Y_{\alpha_0} |\psi\rangle$. Using $|\alpha\rangle\langle\alpha|$, we can consider an Hermitian observable on the environment, which is expressed by

$$\tilde{\mathcal{C}} = \sum_{\alpha} \tilde{g}(\alpha) |\alpha\rangle\langle\alpha|, \quad (\text{S20})$$

where $\tilde{g}(\alpha)$ is any function of α . Since $\langle\Psi_{\star}|\Psi\rangle$ does not depend on the environmental basis, Eq. (13) should hold for $\tilde{\mathcal{C}}$ as well:

$$\left(\frac{\|\tilde{\mathcal{C}}\| + \|\tilde{\mathcal{C}}\|_{\star}}{\langle\tilde{\mathcal{C}}\rangle - \langle\tilde{\mathcal{C}}\rangle_{\star}} \right)^2 \geq \frac{1}{|\text{Tr}_S [e^{\mathcal{K}\tau} \rho_S(0)]|^{-2} - 1}. \quad (\text{S21})$$

$|\alpha\rangle$ can be an arbitrary orthonormal basis in the environment, indicating that the main result of Eq. (13) holds for any continuous measurement.

In the main text, we consider the specific case of $H_{\star,S} = 0$ and $L_{\star,m} = 0$ for all m . Here, the composite state of the conjugate dynamics at $t = \tau$ is $|\Psi_{\star}(\tau)\rangle = |\psi_S\rangle \otimes |0_{N-1}, \dots, 0_0\rangle$, which is unchanged from the initial state. The counting observable \mathcal{C} of Eq. (6) satisfies

$$\langle\mathcal{C}\rangle_{\star} = \langle\Psi_{\star}(\tau)|\mathbb{I}_S \otimes \mathcal{C}|\Psi_{\star}(\tau)\rangle = 0, \quad (\text{S22})$$

$$\langle\mathcal{C}^2\rangle_{\star} = \langle\Psi_{\star}(\tau)|\mathbb{I}_S \otimes \mathcal{C}^2|\Psi_{\star}(\tau)\rangle = 0, \quad (\text{S23})$$

leading Eq. (13) to Eq. (15). For $\tilde{\mathcal{C}}$ defined in Eq. (S20), we have

$$\langle\tilde{\mathcal{C}}\rangle_{\star} = \langle\Psi_{\star}(\tau)|\mathbb{I}_S \otimes \tilde{\mathcal{C}}|\Psi_{\star}(\tau)\rangle \neq 0, \quad (\text{S24})$$

$$\langle\tilde{\mathcal{C}}^2\rangle_{\star} = \langle\Psi_{\star}(\tau)|\mathbb{I}_S \otimes \tilde{\mathcal{C}}^2|\Psi_{\star}(\tau)\rangle \neq 0. \quad (\text{S25})$$

Equations (S24) and (S25) show that

$$\frac{\|\tilde{\mathcal{C}}\|^2}{\langle\tilde{\mathcal{C}}\rangle^2} \neq \frac{1}{|\text{Tr}_S [e^{(-iH - \frac{1}{2}\sum_m L_m^\dagger L_m)\tau} \rho_S(0)]|^{-2} - 1}. \quad (\text{S26})$$

Thus, Eq. (15) depends on how we perform continuous measurement.

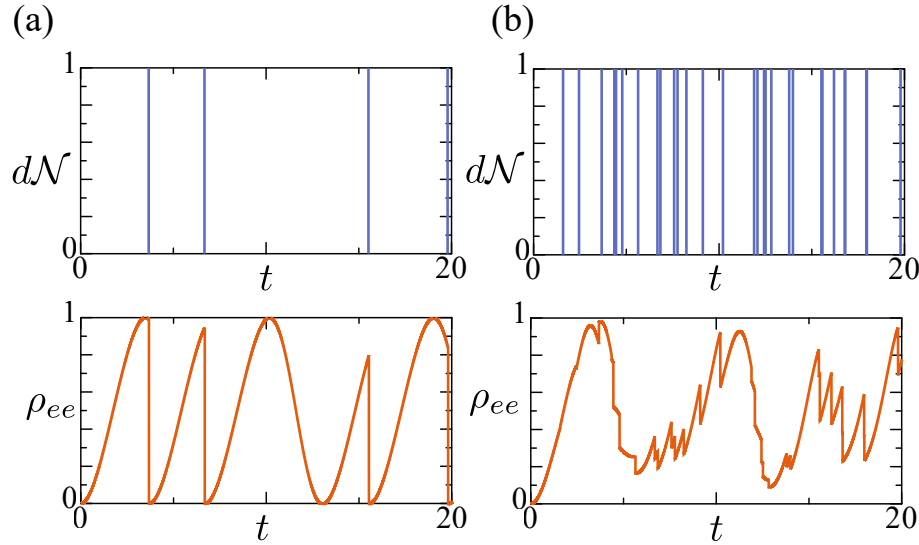


FIG. S1. Quantum trajectories generated by different measurement bases for a two-level atom driven by a laser field (see Section S4 for details). Trajectories are generated by (a) $\zeta = 0$ (corresponding to the measurement basis $\{|0\rangle, |1\rangle\}$) and (b) $\zeta = 1$. The upper panels describe detection of jump events, and the lower panels show the population of the excited state $\rho_{ee} \equiv \langle \epsilon_e | \rho_S | \epsilon_e \rangle$ as a function of t .

S4. NUMERICAL SIMULATION

A. Model

In the numerical simulation, we employ a two-level atom driven by a laser field. As stated in the main text, the Lindblad equation of the system is specified by

$$H_S = \Delta |\epsilon_e\rangle\langle\epsilon_e| + \frac{\Omega}{2}(|\epsilon_e\rangle\langle\epsilon_g| + |\epsilon_g\rangle\langle\epsilon_e|), \quad (\text{S27})$$

$$L = \sqrt{\kappa} |\epsilon_g\rangle\langle\epsilon_e|, \quad (\text{S28})$$

where $|\epsilon_g\rangle$ and $|\epsilon_e\rangle$ denote ground and excited states, respectively, and Δ , Ω , and κ are model parameters. The Kraus operators [Eqs. (3) and (4)] are

$$V_0 = \mathbb{I}_S - i\Delta t H_S - \frac{1}{2}\Delta t L^\dagger L, \quad (\text{S29})$$

$$V_1 = \sqrt{\Delta t} L, \quad (\text{S30})$$

where V_0 and V_1 correspond to no detection and detection of a jump event within Δt , respectively. V_0 and V_1 correspond to the measurement basis of $\{|0\rangle, |1\rangle\}$. Quantum trajectories generated by Eqs. (S29) and (S30) can be described by the following stochastic Schrödinger equation:

$$d\rho_S = -i[H_S, \rho_S]dt + \rho_S \text{Tr}_S [L\rho_S L^\dagger] - \frac{\{L^\dagger L, \rho_S\}}{2}dt + \left(\frac{L\rho_S L^\dagger}{\text{Tr}_S [L\rho_S L^\dagger]} - \rho_S \right) dN, \quad (\text{S31})$$

where dN is a noise increment; $dN = 1$ when a jump event (photon) is detected within dt , and is 0 otherwise. The conditional expectation of dN is given by $\langle dN(t) \rangle = \text{Tr}_S [L\rho(t)L^\dagger]dt$, where $\rho(t)$ is a solution of Eq. (S31).

As shown in Eq. (S21), the main result [Eq. (13)] holds for arbitrary measurements on E . As stated in the main text, the Lindblad equation is invariant under the following transformation:

$$H_S \rightarrow H_S - \frac{i}{2}(\zeta^* L - \zeta L^\dagger), \quad (\text{S32})$$

$$L \rightarrow L + \zeta \mathbb{I}_S, \quad (\text{S33})$$

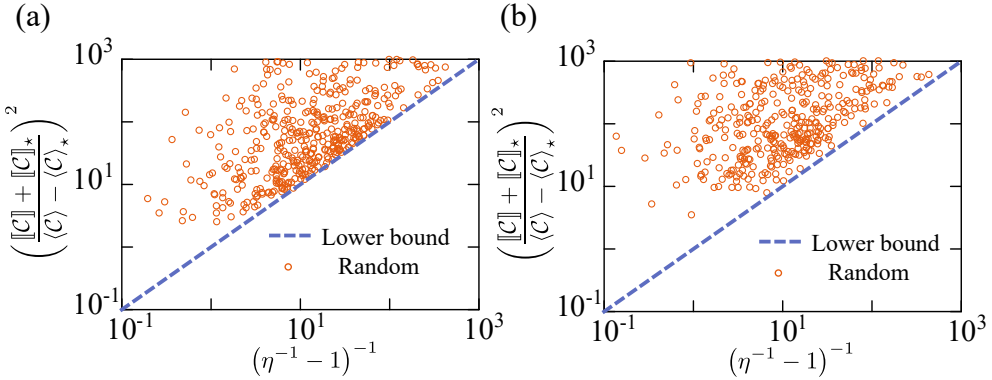


FIG. S2. Precision $(\|C\| + \|C\|_*)^2 / (\|C\| - \|C\|_*)^2$ as a function of $(\eta^{-1} - 1)^{-1}$ for random realizations, where $\eta = |\text{Tr}_S[e^{K\tau}\rho_S(0)]|^2$. Random realizations are plotted by circles and the lower bound by the dashed lines. Random realizations are calculated with (a) fixed continuous measurement V_m and (b) random continuous measurement Y_m by randomly sampling ζ from $|\zeta| \in [0.0, 1.0]$. In (a) and (b), the parameter ranges are $\Delta \in [0.1, 3.0]$, $\Omega \in [0.1, 3.0]$, and $\kappa \in [0.1, 3.0]$ for each of the dynamics, and $\tau \in [0.1, 1.0]$.

where $\zeta \in \mathbb{C}$ can be an arbitrary value. Substituting Eqs. (S32) and (S33) into Eqs. (S29) and (S30), the corresponding Kraus operator is given by

$$\begin{aligned} Y_0 &= \mathbb{I}_S - i\Delta t \left[H_S - \frac{i}{2}(\zeta^* L - \zeta L^\dagger) \right] - \frac{1}{2}\Delta t (L^\dagger + \zeta^*) (L + \zeta) \\ &= \mathbb{I}_S - i\Delta t H_S - \zeta^* L \Delta t - \frac{1}{2}\Delta t (L^\dagger L + |\zeta|^2), \end{aligned} \quad (\text{S34})$$

$$Y_1 = \sqrt{\Delta t} (L + \zeta \mathbb{I}_S), \quad (\text{S35})$$

where Y_0 and Y_1 correspond to no detection and detection of a jump event, respectively. Y_0 and Y_1 [Eqs. (S34) and (S35)] and V_0 and V_1 [Eqs. (S29) and (S30)] are related through a unitary transformation shown in Eq. (S17), where \mathcal{B} is given by

$$\mathcal{B} = \begin{bmatrix} -\frac{1}{2}|\zeta|^2\Delta t + 1 & -\sqrt{\Delta t}\zeta^* \\ \sqrt{\Delta t}\zeta & -\frac{1}{2}|\zeta|^2\Delta t + 1 \end{bmatrix}. \quad (\text{S36})$$

We have shown that the measurement basis is transformed through Eq. (S18), where $\mathcal{A} = \mathcal{B}^\dagger$. Since Eq. (S36) shows that we can specify \mathcal{B} through ζ alone, we can change the measurement basis by changing ζ . Figure S1 shows trajectories generated by (a) $\zeta = 0$ and (b) $\zeta = 1$. As explained above, the trajectories of (a) and (b) in Fig. S1 use different measurement bases. Although the trajectories of (a) and (b) in Fig. S1 are different, both cases reduce to the same dynamics on average.

B. Simulation of Eq. (13)

We conduct a numerical simulation to verify Eq. (13). Equation (13) considers two dynamics, the original and its perturbed dynamics. For each of the dynamics, we randomly select the model parameters Δ , Ω , and κ (that is, 6 model parameters in total). The time duration τ is randomly sampled (see the caption of Fig. S2 for the parameter ranges), and the initial density operator ρ_S is also determined randomly. For the selected parameters and density operator, we generate different quantum trajectories and calculate $(\|C\| + \|C\|_*)^2 / (\|C\| - \|C\|_*)^2$. In Fig. S2(b), we plot $(\|C\| + \|C\|_*)^2 / (\|C\| - \|C\|_*)^2$ as a function of $(\eta^{-1} - 1)^{-1}$ with $\eta = |\text{Tr}_S[e^{K\tau}\rho_S(0)]|^2$ (which is the right-hand side of Eq. (13)) by circles, where the dashed line denotes the lower bound. All circles are located above the line, verifying Eq. (13) for the driven two-level atom system.

As denoted above, Eq. (13) should hold for any continuous measurement (any unraveling). Besides, we conduct a numerical simulation for different continuous measurements. First, we randomly determine ζ to change the continuous measurement. Then, we follow the same procedure as in Fig. S2(a). In Fig. S2(b), we plot $(\|C\| + \|C\|_*)^2 / (\|C\| - \|C\|_*)^2$ as a function of $(\eta^{-1} - 1)^{-1}$ with $\eta = |\text{Tr}_S[e^{K\tau}\rho_S(0)]|^2$ by circles, where the dashed line denotes the lower bound of Eq. (13). All circles are above the line, verifying Eq. (13) for different continuous measurements.

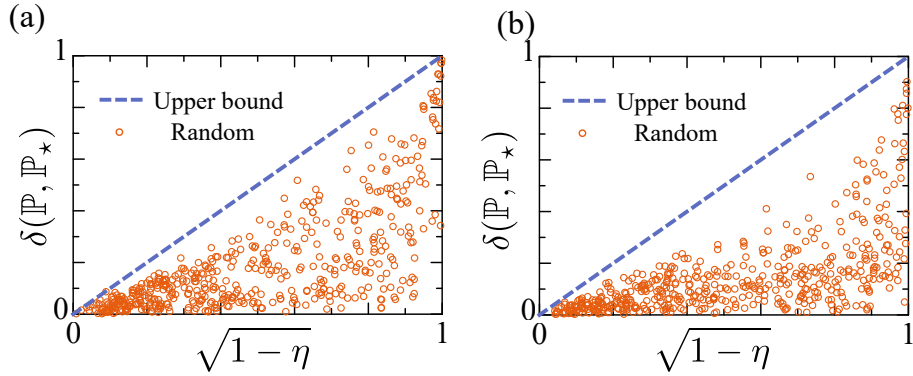


FIG. S3. Total variation distance $\delta(\mathbb{P}, \mathbb{P}_*)$ as a function of $\sqrt{1 - \eta}$ for random realizations, where $\eta = |\text{Tr}_S[e^{\kappa\tau}\rho_S(0)]|^2$. Random realizations are plotted by circles and the upper bound by the dashed lines. Random realizations are calculated with (a) fixed continuous measurement V_m and (b) random continuous measurement Y_m by randomly sampling ζ from $|\zeta| \in [0.0, 1.0]$. In (a) and (b), the parameter ranges are $\Delta \in [0.1, 3.0]$, $\Omega \in [0.1, 3.0]$, and $\kappa \in [0.1, 3.0]$ for each of the dynamics, and $\tau \in [0.1, 10.0]$.

C. Simulation of Eq. (18)

Next, we conduct a numerical simulation for Eq. (18). Following a similar approach in Fig. S2(a), for each dynamics, we randomly select the model parameters Δ , Ω , and κ (6 model parameters in total). The time duration τ is randomly sampled (see the caption of Fig. S3 for the parameter ranges), and the initial density operator ρ_S is also determined randomly. For the selected parameters and density operator, we generate different quantum trajectories and calculate $\delta(\mathbb{P}, \mathbb{P}_*)$. In Fig. S3(a), we plot $\delta(\mathbb{P}, \mathbb{P}_*)$ as a function of $\sqrt{1 - \eta}$ with $\eta = |\text{Tr}_S[e^{\kappa\tau}\rho_S(0)]|^2$ by circles, where the dashed line denotes the upper bound. All circles are located above the line, verifying Eq. (18) for the driven two-level atom system.

Thus, Eq. (18) should hold for any continuous measurement (any unraveling). We also conduct a numerical simulation for different continuous measurements in Eq. (18). The basic setting is the same as in Fig. S3(a), and we follow the same procedure as in Fig. S2(b) to change the measurement basis. In Fig. S3(b), we plot $\delta(\mathbb{P}, \mathbb{P}_*)$ as a function of $\sqrt{1 - \eta}$ with $\eta = |\text{Tr}_S[e^{\kappa\tau}\rho_S(0)]|^2$ by circles, where the dashed line denotes the upper bound of Eq. (18). All circles are above the line, verifying Eq. (18) for different continuous measurements.

[1] G. T. Landi, *Quantum Information and Quantum Noise*, Tech. Rep. (University of São Paulo, <http://www.fmt.if.usp.br/~gtlandi/quantum-information-and.html>, 2018).